NAVAL RESEARCH REVIEWS

OCTOBER 1972

DEPARTMENT OF THE NAVY
OFFICE OF NAVAL RESEARCH

PROFILES IN SCIENCE

Dr. William A. Nierenberg

Dr. William A. Nierenberg, Director of Scripps Institution of Oceanography, has been associated with the University of California since 1950. He is primarily known for his work in low-energy nuclear physics and has established himself as a leading expert in the field of underwater research and warfare. On leave from the University in 1953 and 1954, he served as a Project Director of Columbia University's Hudson Laboratories which were engaged in oceanographic and underwater sound studies.

Dr. Nierenberg's interests have led him into international affairs. From 1960 to 1962, he served in Paris as Assistant Secretary General of NATO for Scientific Affairs and was at the same time Professeur Associe at the University of Paris. He was a member of the working group for an International Institute of Science and Technology and has been active in establishing exchange programs with Middle Eastern universities.

He has directed productive research in the field of atomic beam measurements of electronic and nuclear properties of radioactive atoms, and has written more than 100 publications in this field. Recently the President appointed Dr. Nierenberg Chairman of the National Advisory Committee on the Oceans and Atmosphere. For many years Dr. Nierenberg has been closely associated with the Office of Naval Research.

Electric Currents Hasten Bone Fracture Healing

C. T. Brighton*
University of Pennsylvania, Philadelphia

The first documented evidence that electric currents promote bone fracture healing in humans has been established by a Navy study.

This study was conducted by the University of Pennsylvania Medical School in conjunction with the Philadelphia Naval Hospital. It was supported by the Bureau of Medicine and Surgery under a contract with the Office of Naval Research.

The evidence that electric currents are beneficial to the healing process of bones was obtained through experiments first with animals, then with humans. The studies proved conclusively that electric currents promote fracture healing.

It had been known for some time that electrical charges play a role in bone growth and healing. Previous investigation, however, had been inconclusive because of the problem of delivering a constant current to the bone. Current provided to the bone decreased as tissue resistance developed. The investigators in the Navy research study solved the problem by developing a compact power pack designed to deliver a steady current up to one hundreth of an ampere. The tiny power pack is implanted under the skin, with the negative electrode secured directly across the fracture and the positive electrode in a nearby location.

One experiment to test bone reaction to varying amounts of direct current involved the use of adult male white New Zealand rabbits, weighing between 2 and 4 kilograms. An implant (power pack) with field-effect transistors and resistors was built to deliver a constant current, regardless of changing resistances in the tissues (Figure 1). The circuit was sealed in a methacrylate capsule from which protruded a stainless steel cathode and anode as well as lead wires for monitoring the current.

After anesthesia was administered, the surface of the shaft of the right femur was exposed beneath the fibrous periosteum of the bone to afford a better view. Two holes were drilled in the femoral shaft for the insertion of the cathode and anode protruding from the encapsulated power

*Dr. Carl T. Brighton is Assistant Professor of Orthopaedic Surgery and Director of Orthopaedic Research at the University of Pennsylvania School of Medicine, Philadelphia, Pennsylvania. Dr. Brighton has done outstanding work in the field of academic orthopaedic surgery and while serving as Orthopaedic Surgeon in the Philadelphia Naval Hospital, he received the Navy's Meritorious Service Award.

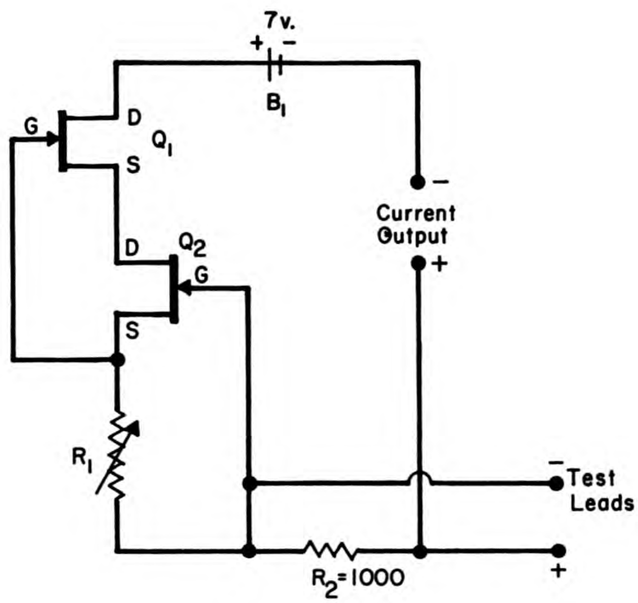

$R_1 = 3 \times 10^6 \Omega$ for $1 \mu A$ output
$8 \times 10^5 \Omega$ for $5 \mu A$ output
$4 \times 10^5 \Omega$ for $10 \mu A$ output
$15 \times 10^4 \Omega$ for $20 \mu A$ output

Figure 1 – Circuit of power pack shows the specific resistor, R_1, necessary for each amperage level constant current source. Q_1 and Q_2 are field-effect transistors.

pack. The power pack was further secured to the bone by two silk ligatures. The monitor wires used to measure the current during the experiment were advanced subcutaneously and brought out through the skin of the rabbit. The current delivered by the power pack was also measured directly from the electrodes at the time of the insertion and removal. The constant currents selected for use were 1, 5, 10, 20, 50 and 100 microamperes.

On the tenth postoperative day, the rabbit was sacrificed, the femur and power pack were excised, and the bone was immediately placed in neutral-buffered formalin to be preserved for future observation. X-ray pictures of the fracture were taken in several views, using fine grain industrial x-ray film. The bone samples were then decalcified, sectioned in a plane perpendicular to the longitudinal axis of the electrodes, and stained with hemotoxylin and eosin to provide better viewing. For control experiments, methacrylate cylinders with stainless steel prongs were inserted into similar rabbits under sterile conditions and the aforementioned procedures were followed except that no current was passed between the electrodes.

Specimens that were included in the results were free of infection and fractures and had power packs that maintained at least 75 percent of their original current for the full ten day period. Forty-six rabbits met these conditions and were used as experimental subjects. They included six control rabbits, nine rabbits at 1 microampere, six at 5, 10, 20 and 100 microamperes and seven at 50 microamperes.

On gross inspection, the control rabbits and those in the 1 and 5 microampere groups showed little reaction at either the anode or cathode implant sites. The rabbits subjected to 10 and 20 microamperes displayed a dark discoloration around the anodal site but no apparent reaction in the vicinity of the cathode. At 50 and 100 microamperes, marked discoloration occurred at both electrode sites.

Microscopically, bone formation occurred predominantly around the cathode. The optimum range of current for such formation was 5 to 20 microamperes with diminution of bone production above 20 microamperes. Microscopic sections showed the amount of bone cartilage, and fibrous tissue regeneration as well as tissue destruction at the anode and cathode with different currents. At all current magnitudes, tissue destruction was present at the anode and was severe at 20 microamperes or more (Figure 2). This reaction was the most consistent

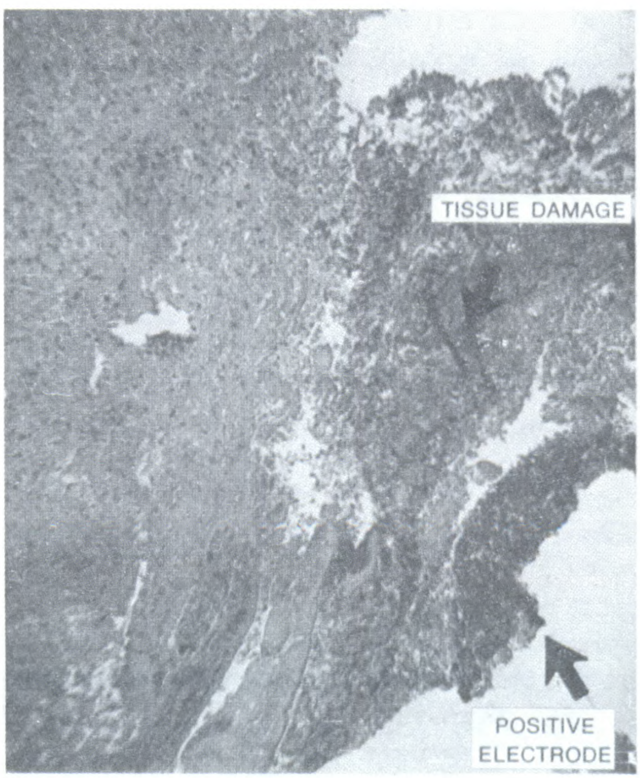

Figure 2 — Area adjacent to positive electrode delivering 100 microamperes shows massive electrocoagulation of tissue. Hematoxylin and eosin, ×80.

microscopic finding. At the cathode, however, severe destruction did not occur until 100 microamperes were applied (Figure 3).

Bone formation was increased over that of controls between 5 and 20 microamperes at the cathode implant, but the increase was only moderate. The production of fibrous tissue and cartilage was minimally increased at the cathode in this range (Figure 4).

These experimental observations that electric currents did indeed promote healing in animals led to the use of electric currents on the fractured ankle of a 51 year old woman. The fracture had been reduced closed and the leg placed in a long cast for 13 weeks. Weight bearing was begun at 15 weeks. The patient did not return for follow-up, but walked with assistance for one year suffering intermittent pain and swelling. In February, 1971, she returned to the hospital because of an increase in pain and swelling and it was found that the fracture had failed to re-unite.

The patient was moderately obese, but in good health aside from the fracture defect of the right ankle (Figure 5). She agreed to the use of

Figure 3 — Adjacent to negative electrode delivering 100 microamperes, no new tissue formation, and necrotic soft tissue and bone are seen. Hematoxylin and eosin, ×80.

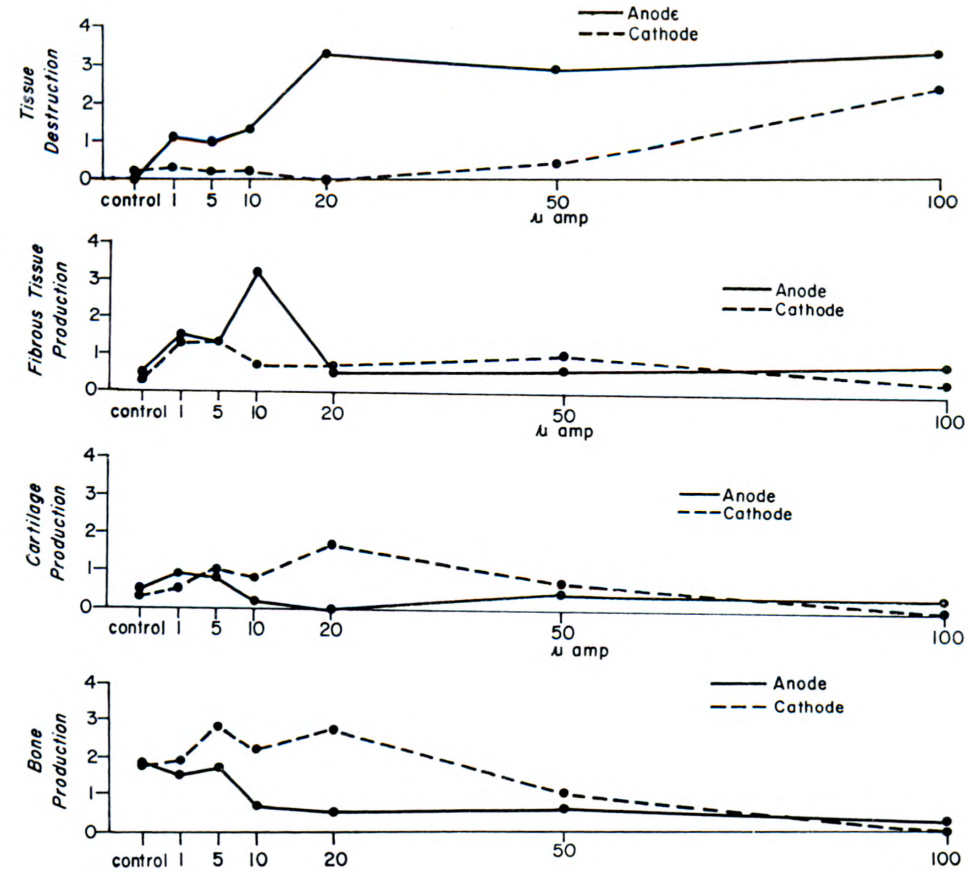

Figure 4 — Mean values of amounts of tissue production and destruction are shown for each current level studied

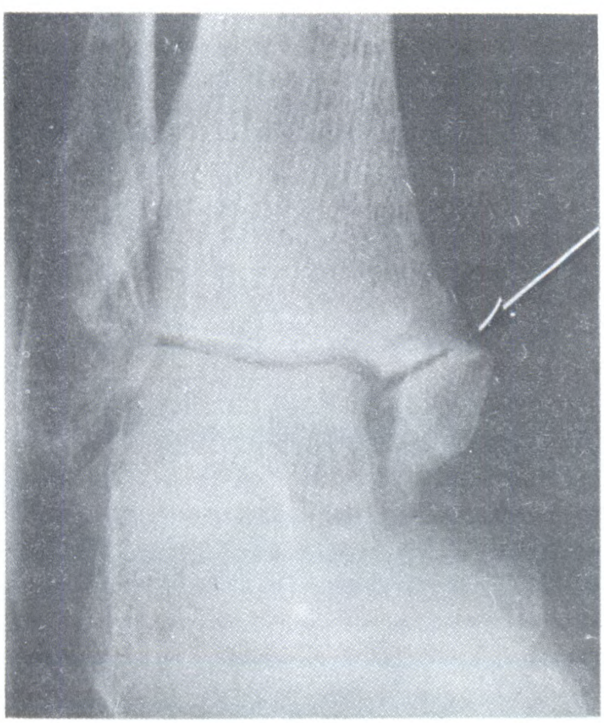

Figure 5 — Roentgenogram of the patient's right ankle showing a healed fracture of the lateral malleolus and a nonunion of the medial malleolus

the electrical stimulation technique after a full explanation of the problem. On February 23, 1971, she was taken to the operating room where, under local anesthesia, a 2 cm. incision was made over the non-union site. A straight needle was used to open a small hole in the fracture defect with minimal soft tissue disturbance. The cathode, a 26 gauge stainless steel wire, was introduced through a separate stab incision, placed within the fracture defect (see Figure 6) and fastened to the surrounding tissue with a suture. The anode, an aluminum grid, was placed over the skin of the foot. The power pack was fixed to a short

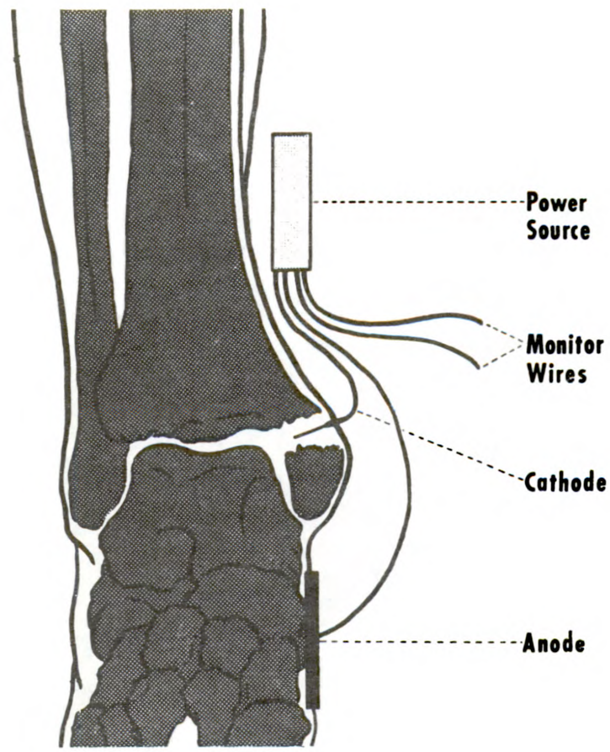

Figure 6 — Drawing depicting the insertion of the cathode into the nonunion site of the medial malleolus. The anode is applied to the surface of the skin, while the power source is attached to the short leg cast. The technique used in delivering electric current to bone involves inserting a wire cathode into the bone at the fracture site, under local anesthesia. The wire is attached to the power source, a 7.5-volt battery with resistors and field-effect transistors designed to produce a constant current of 10 microamperes. The anode, an aluminum grid, is placed on the skin. A short non-weight bearing cast is applied to the leg, and the wires from anode and cathode are brought out through a window in the cast. The battery pack is strapped to the cast.

leg cast which also secured the wires leading to both electrodes. Monitoring wires exited through the cast.

The current delivery was checked daily and later weekly. At no point during the treatment did the current vary more than 2 microamperes. When the cast was changed after 3 weeks, the fracture site was non-tender and mobility of the fragment could no longer be detected. The patient was kept non-weight-bearing in the short leg cast for nine weeks. The wire and power pack were then removed and the patient was placed on crutches with partial, and two weeks later, full weight bearing. She has had no further symptons and developed no problems from the wire insertion. X-rays revealed union of the fracture (Figure 7).

These experiments and others with both animals and humans have substantiated the belief that electric currents hasten bone healing. The observations strongly suggest that the optimum direct current for new bone formation is in the range of 5 to 20 microamperes. The effects of the currents on tissue show that the longer currents caused no damage, while the high currents destroyed tissue at both the anode and cathode sites. It is unlikely that currents below 5 microamperes would be more effective in stimulating bone tissue.

Figure 7 — Roentgenogram of the patient's right ankle after discontinuation of current that had flowed for 9 weeks. The nonunion of the medial malleolus is healed.

Although this research is in the developmental stage, two other patients are undergoing similar treatment. Further success would suggest that the technique might replace some bone grafting. It offers hope for halving the healing time of some fractures. Investigations are being conducted to further determine the best amperage and cathode surface area that might help to heal more complicated fractures with larger bone defects.

Ecology Research in Arctic

A team of Naval Research Laboratory scientists were aboard the oceanographic research vessel, USNS MIZAR, in Arctic waters during September of this year to conduct experiments concerning the ecology of the area.

The scientific mission was to study the concentration of toxic trace elements in the Arctic's atmosphere, fog, ice and seawater.

As a result of measurements of mercury in the atmosphere, sea ice and mercury profiles in seawater in an Arctic experiment last year, an NRL team found indications that sea ice is an important reservoir for the toxic element in the geochemical cycle.

The experiment further indicated that atmospheric mercury is in some way transferred to sea ice, perhaps by the condensation and deposition of fog.

The scientists concentrated their efforts on the microphysics of the fog by incorporating instrumentation for obtaining the droplet size distribution, the droplet surface area, the mean electrical charge carried by the droplets, and the saturation in the air about the droplets.

NRL-developed equipment for these measurements, mounted on the USNS MIZAR, were in the ice field under conditions which are ideal for obtaining advection (the horizontal movement of air masses that causes changes in temperature of physical properties) fog. Advection fog is produced by nature causing warm air, such as off the Norwegian current, to be brought abruptly over cold sea surfaces supplied by the ice field.

NRL has developed a unique multidiscipline approach for tracing air masses and examining the basic mechanisms involved in the life cycle of Arctic advection fogs. The study combines atmospheric chemistry, atmospheric radio chemistry, and atmospheric electricity, as well as meteorological techniques to determine the true sequence of events taking place in an advective fog.

Unique Wind-Wave Tank

A wind-wave tank 58 feet long and 4 feet wide which is capable of producing the equivalent of 50-knot winds at sea has been constructed at the Naval Research Laboratory.

It is known that short gravity and capillary waves scatter radar impulses at the ocean surface and that the spatial and temporal distributions of these scatterers are influenced by many factors, including the wind and the structure of the larger waves.

(Continued on Page 20)

Density Gradients at River Mouths

J. M. Coleman, L. D. Wright, and J. N. Suhayda*
Coastal Studies Institute
Louisiana State University

Freshwater effluents from river outlets spread and diffuse into ambient marine water; the interactions which take place between these water masses at and immediately seaward of the river mouth are critical in controlling the dissemination of sediment and water transported by the river. Mixing between these water masses, each characterized by differing properties, takes place in many ways and is affected by various mechanisms. These mechanisms control the outflow patterns and hence fundamentally determine the pattern of sediment dissemination, accumulation, and distribution of the bars that form at river mouths. Thus greater understanding of the behavior of the effluent plume would significantly aid charting, navigation, and similar operations in these constantly changing areas of strategic importance. In addition, several types of density gradients occur between the water masses which drastically affect acoustical transmission and reflections in various search operations, swimmer defense techniques, and mining operations. If the density contrasts are understood, they can be favorably utilized as an acoustical barrier for hiding or to provide safe upstream penetration for swimmers. The Office of Naval Research is sponsoring this project.

For the past several years, scientists at the Coastal Studies Institute have been studying the processes of river outflow in various world deltas. These studies have involved extensive field observations of flow and density structure and analyses of various types of remote sensing imagery. It was found that river outflow patterns are significantly affected by a variety of local processes such as tide, waves, and river discharge but that effluent spreading and diffusion tendencies are governed most strongly by density contrasts. The density gradients are a function of salinity, temperature, and turbidity differences between the two water masses. The cover picture shows a high-altitude (20,000 meters) photograph of some of the mouths of the Mississippi River. The original photograph was exposed on color infrared film with a 510μ filter but has been reproduced in conventional black and white.

*Dr. Coleman is Associate Professor and Assistant Director of the Coastal Studies Institute at Louisiana State University. Dr. Wright is Assistant Professor and Research Associate at the Coastal Studies Institute. Dr. Suhayda is Assistant Professor at Louisiana State University. The Institute which was established in 1954 under the sponsorship of ONR pursues research on sea-air-land interaction systems, and assess the range and combinations of process-response variability along the world coasts.

486-913 O - 72 - 2

Note that several distinct water masses (labeled on the photo) are apparent on the image; these can be attributed predominantly to turbidity, but each boundary also displays salinity and temperature differences. Figure 1 is a tracing made from a scanning isodensitometer of a part of this photograph, and water mass boundaries have been outlined and labeled for illustrative purposes. Seven distinct water masses can be identified in the region of South Pass, Mississippi River. The water masses labeled "a" (Figure 1) are small, fresh, highly turbid effluent plumes emanating from the numerous breaks in the main river channel and debouching into the adjacent shallow-water bays. The major freshwater effluent plumes are labeled "b" from South Pass, "d" from Southeast Pass, and "e" from Northeast Pass. These water masses are low in salinity and are highly turbid. The slow-moving, thin,

Figure 1 — Tracing from a scanning densitometer record of a high-altitude (20,000 meters) color infrared image (510μ filter) taken of South Pass during May 1972. The cover photograph is the original from which the densitometer trace was made. Water mass boundaries are outlines and labeled to emphasize their patterns. The characteristics of the water masses are described in the text.

and highly stratified band of ambient fresh to brackish turbid water labeled "c" originates in the shallow bays between the major passes. Often it is quite warm because of constant mixing by wave action and is distinct in thermal imagery. The water mass labeled "f" is less turbid, slightly diluted (salinity 25 °/₀₀ – 30 °/₀₀) coast marine water drifting from east to west. The clear gulf saline water mass is designated "g" in Figure 1.

Density gradients (including differences in salinity, turbidity, and temperature) exist at the boundary of each water mass and form a complex maze of interfaces in plain view, as well as each having a vertical structure that varies in thickness spatially and temporally. Let us examine some of the major interfacial boundaries and see what properties they possess and how they might affect operations in and near river mouths.

Salt Wedge River Intrusion

On the basis of the degree to which the discharging fresh water mixes with the undiluted seawater, three main types of circulation in river mouths are recognized: (1) well-mixed river mouths, in which salinity exhibits little or no vertical variation; (2) partially mixed river mouths, which lack steep gradients but have a large vertical range of salinity around the mean; and (3) highly stratified river mouths, where freshwater and saltwater layers are separated in the vertical by a well-defined interface (1,2). It is this latter type, the highly stratified salt wedge, that posess potential operational problems. When the average velocity of a discharging stream is below a critical value, the density differential between river water and seawater enables seawater to underflow the fresh river water and proceed upstream to some point where shear stress at the salt wedge interface balances hydrostatic pressure arising from the density contrast. Several river deltas, including the Mississippi (USA), Po (Italy), Chao Phyra (Thailand), Danube (Romania), Han (Korea), and Mekong (Vietnam), satisfy the requirements for the highly stratified situation, and salt wedges proceed upstream in the river channels. Figure 2A is a longitudinal section down one of the distributary channels of the Mississippi River during low river stage flooding tide, showing the water masses and velocity distribution patterns. Flow is downstream at all depths upstream from the toe of the wedge (kilometer 0 to kilometer 5.0). Upon encountering the toe of the salt wedge, seaward flow is concentrated above the interface, while upstream flow exists within the wedge. Upstream velocities within the salt wedge can attain speeds of up to 1.0 meter per second during flooding tide.

Low river gradients of the distributaries result in tidal phases which have a significant influence on the hydrostatic gradient and hence on the movement and interfacial characteristics of the salt wedge. Figures

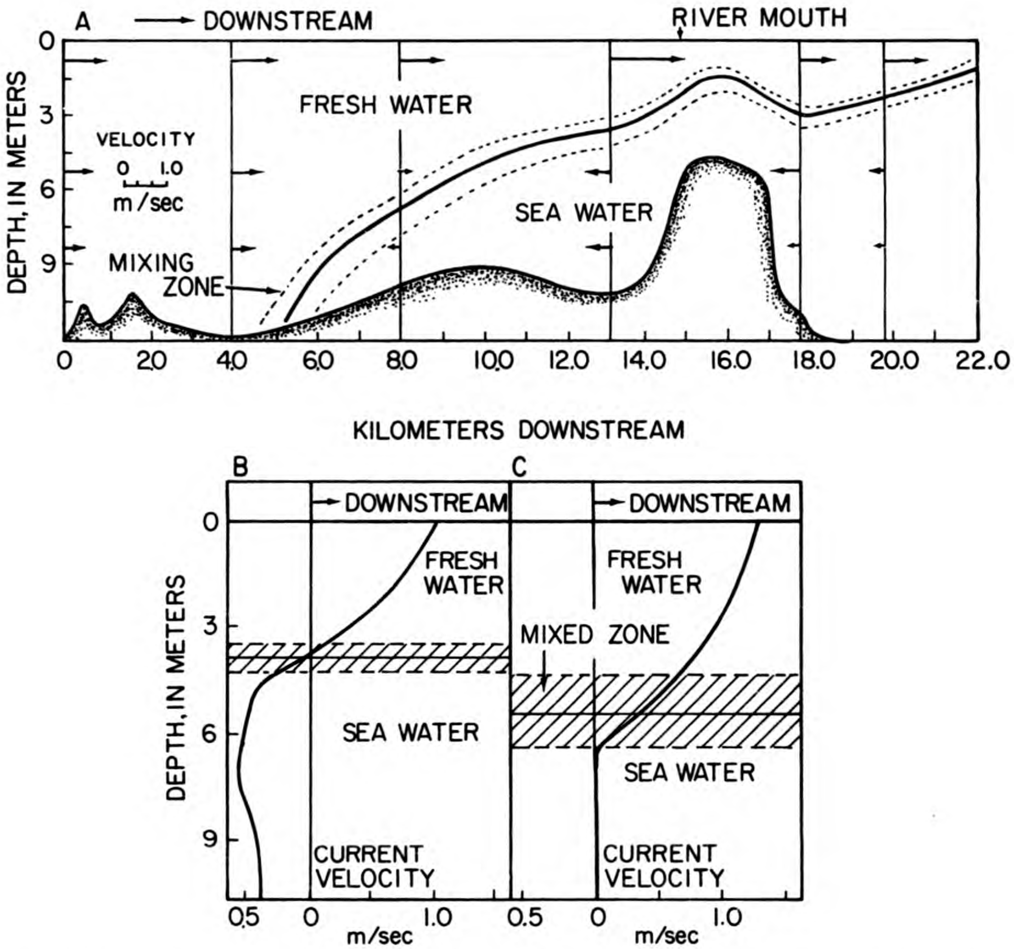

Figure 2 — A—Longitudinal profile of South Pass, Mississippi River, during low stage illustrating the salt wedge intrusion. B and C—Velocity profiles at station kilometer 13 during flooding tide (B) and ebbing tide (C).

2B and C show typical low-stage stratification situations and current profiles for flooding (Figure 2B) and ebbing (Figure 2C) tides at station kilometer 13. During the flooding phases, the interface is quite sharp (thin zone of mixing) and downstream velocities in the fresh water decrease progressively with depth from a maximum of 1.0 meter/sec at the surface to a null point at the interface (depth of 4.1 meters below the surface). Below the interface, flow is directed upstream and in this instance reaches a velocity of only 0.5 meter/sec. During the ebbing phase (Figure 2C), surface flow is considerably swifter, attaining a velocity of some 1.5 meter/sec, and is directed downstream only. The interface is much more diffuse, and the maximum density gradient is located at 6 meters below the surface. Within the salt wedge, velocities are essentially zero; however, quite often the velocity within the salt wedge will reverse itself and flow downstream at speeds as high as 0.8 meter/sec.

Thus, in a salt wedge river mouth, density gradients occur in the river channels, where salt water underflows the fresher river water. In the Mississippi River, river water during low stage has an average temperature of some 18°C, whereas the saline gulf water has a temperature of 21°C. Thus a temperature gradient is also represented at the interface. River water has a suspended sediment concentration that varies from in excess of 500 mg/1 to less than 40 mg/1 near the river mouth. Gulf waters, on the other hand, are normally lower and average some 20 mg/1. Observations indicate that the interface within the channel marks a turbidity maximum. River water is quite turbid in comparison to the underlying saline water, but maximum turbidity was found to occur immediately at the interface, so that the interface also marks sharp turbidity contrasts.

The depth of the interface, the sharpness of the interfacial gradients, and velocity profiles vary with tidal phase and river stage. Figure 3 is a reproduction of a fathometer record of acoustical reflections from the interface which were recorded on a Raytheon fathometer. In many cases, interfacial gradients are so sharp during flooding tide that the bottom trace is completely lost, especially when made from a moving ship. Charting and acoustical searches, therefore, should be planned during ebbing phase, when interfacial boundaries are less intense. Ships negotiating river mouths often encounter a "dead water" effect

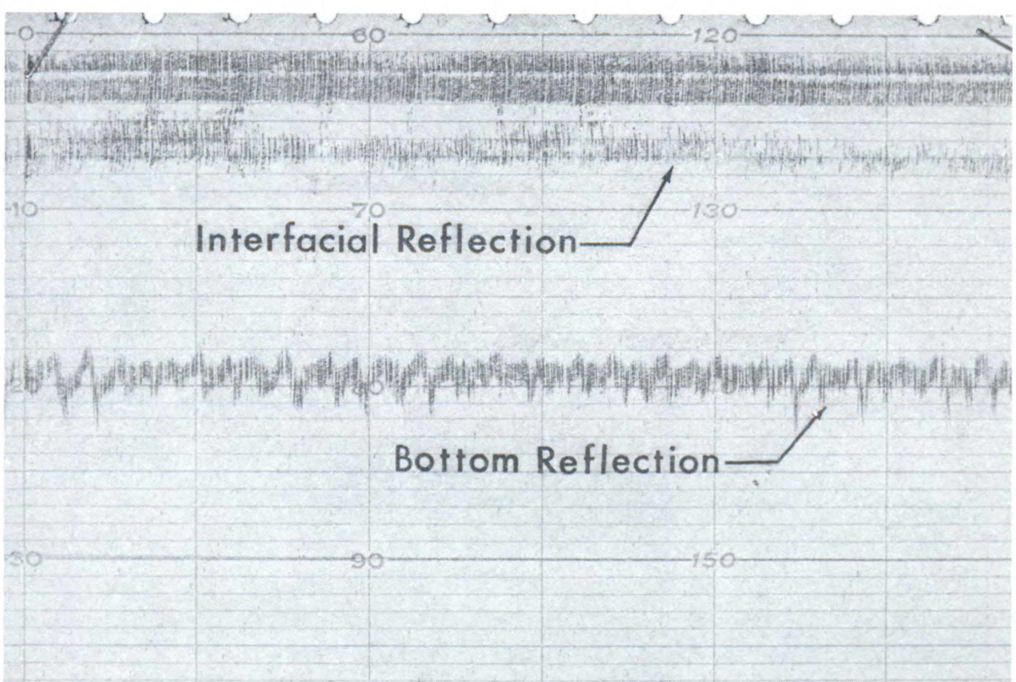

Figure 3 — Reproduction of a fathometer trace showing acoustical reflections from the interface between the freshwater and saltwater wedge

whereby they experience a loss of power. This occurs when the depth of the ship's keel coincides with the depth of the interface, a situation which results in the generation of interfacial waves. The drain on the ship's power is proportional to the power required to generate the internal waves. Salt wedges could therefore be detrimental to operations but, on the other hand, SCUBA divers could utilize the interface as an acoustical blind zone, as well as take advantage of the upstream-directed currents to penetrate inland via the river mouth.

Outflow Effluent Plumes

Once the effluent leaves the confines of the channel, other mechanisms exert control on its pattern and structure. Mixing between the river and saline water has been regarded as a purely lateral phenomenon that approximates a free turbulent plane jet expanding above the freshwater-saltwater interface (3). Recent studies (4,5), however, have shown that the river plume does not behave as a turbulent plane jet but rather expands seaward as a laterally homogeneous layer above the underlying salt water, and seaward flow deceleration and freshwater deconcentration result primarily from vertical mixing across the interface, in particular as a result of interfacial waves. Outflow velocity and depth of the freshwater-saltwater interface at the mouth tend to maintain a relationship which reflects a balance between seaward inertia and laterally directed buoyant forces. Figure 4 is a generalized diagram illustrating the three-dimensional aspect of the effluent plume, including buoyant spreading and interfacial mixing. At any given time, plume geometry and orientation and the degree of vertical mixing may be significantly modified by marine agencies such as tides, winds, coastal currents, and waves.

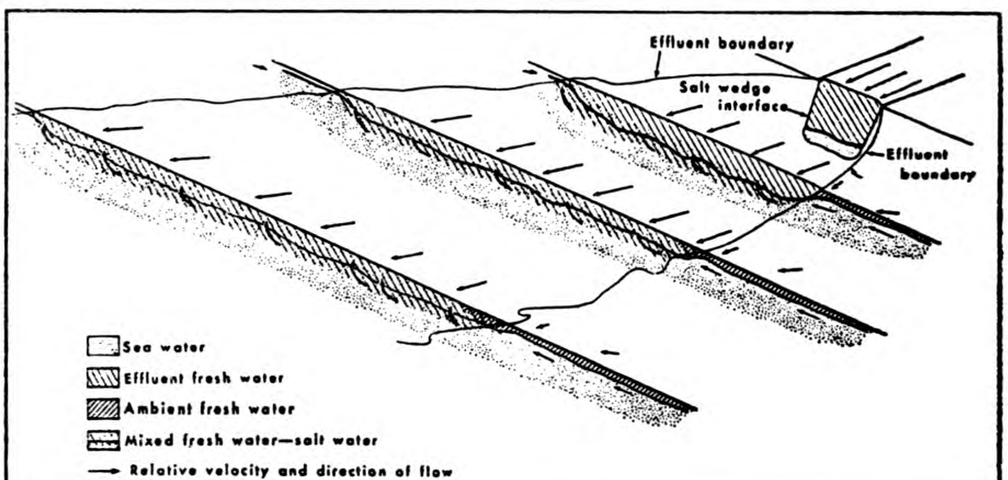

Figure 4 – Generalized diagram illustrating buoyant spreading and interfacial mixing of an effluent river plume

Figure 5 is a Reconofax IV thermal scanner image (8-14μ spectral band) taken at night of the South Pass, Mississippi River, effluent during flooding tide. This sensor enhances water mass contrasts on the basis of temperatures and by gray tones indicates mixing phenomena. Lighter tones indicate warmer temperatures. Precision radiation thermometer data indicate approximate average temperatures of 18°C and 21°C for river water and seawater, respectively. The sand beach (a) is dark, indicating the low emission of heat from the cool sand. The river mouth of South Pass (b) is jettied, and the jetties show up as heat sources. At the river mouth, surface water temperature is comparable to that of the adjacent ambient fresh-brackish water. Note that as the flow leaves the river channel there is an abrupt lateral expansion resulting from buoyant forces. Seaward of this point, expansion rates diminish and the plume is deflected west because the flood tide current is directed east to west. Temperatures within the plume tend to increase seaward and eventually approach that of the gulf water (not shown in this image). Temperature within the ambient fresh-brackish water, on the other hand, remain constant in a seaward direction. Transverse to the effluent axis, temperatures at any given distance seaward are relatively uniform, illustrating the importance of vertical interfacial mixing and the comparative insignificance of lateral mixing. The most striking density gradient is found along the eastern boundary of the plume (c), where temperature differences of 2°C-3°C occur over a rather narrow zone. Turbidity contrasts are not as striking because the ambient fresh-brackish water is also turbid. Salinity contrasts near the mouth are quite high: 1 ‰ in the plume and 10 ‰ in the ambient fresh-brackish water. As a result of vertical mixing between the effluent and the underlying saline water, surface salinities within the plume increase seaward. Within a short distance of the river mouth, salinities in the plume exceed those of the flanking water mass. This vertical mixing is evident in Figure 5 as the temperatures within the plume become warmer (lighter tones) than the adjacent water mass by mixing with the warmer underlying saline water. The most intense mixing between the river water and the underlying saline water occurs over a narrow zone (labeled "d" in Figure 5) that is normally located four channel widths seaward of the mouth. This position corresponds to the crest of the river mouth bar and to the position at which the salt wedge interface rises to its shallowest depth (see Figure 2A).

The overall plume of South Pass can be traced as a discrete water mass for some 5 to 7 km from the river mouth. Near the mouth, the plume thickness varies between 3 and 5 meters and gradually diminishes to only 0.5 to 1 m near its seaward end. The surface plume pattern at any given time is controlled primarily by tidal phase and wind direction. Tides propagate along the Louisiana coast from east to west; and, during flooding tide, the plume is deflected strongly to the west. During ebbing

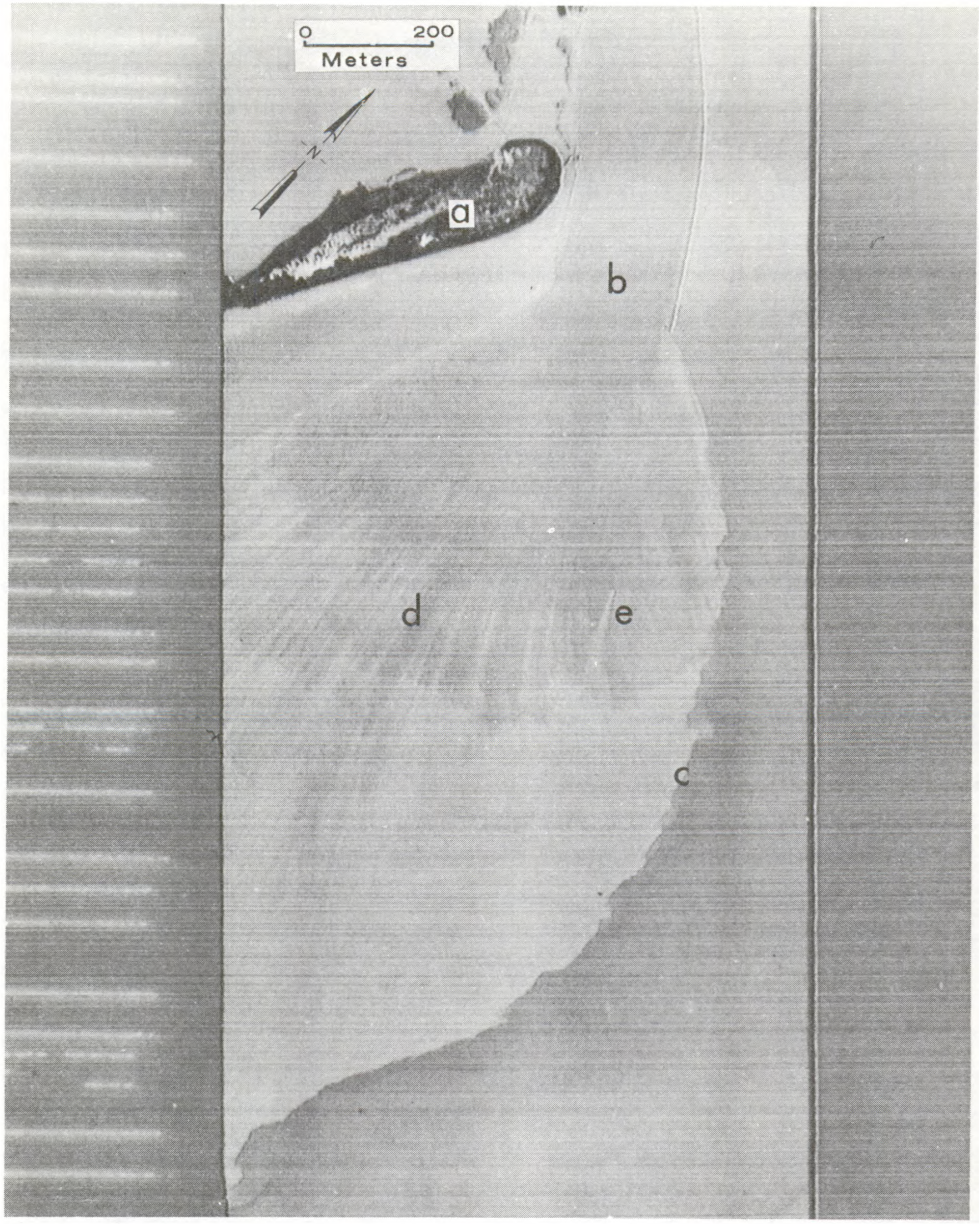

Figure 5 — Reconofax IV thermal infrared scanner image (8-14μ spectral band) taken during flooding tide at night of the South Pass effluent plume. Lighter tones correspond to warmer temperatures. a—Cold sand beach; b—jettied river mouth; c—sharp density gradient along eastern plume boundary; d—zone of intense vertical mixing; e—wake behind navigational buoy.

tide, deflection is considerably less and the plume displays a rather symmetrical seaward expanding pattern. Strong onshore winds will also cause the plume to be significantly deflected, and a strong westerly wind, combined with an ebbing tide, will occasionally result in the plume's being deflected eastward from the channel mouth. Figure 6 is a higher altitude (5,000 meters) RS14 thermal scanner image (8-14μ spectral band) of the entire plume taken at 1600 hours during ebbing tide. As can be seen, the distribution and pattern of density gradients associated with river plume are complex and display differing degrees of sharpness. Let us examine some of these density gradients and describe their nature and structure.

The water mass labeled "a" represents cold river water issuing through the numerous breaks or "crevasses" of the channel into adjacent warm, shallow, fresh-brackish water bays. These plumes are very thin, rarely exceeding 1.5 m in thickness. Because of the large differences in water temperature, however, interfaces are quite sharp and would drastically affect acoustical transmission and reflection. Turbidity and salinity differences are not so contrasting as those associated with the main river plume. The water mass labeled "b" in Figure 6 is the main effluent plume of the South Pass distributary. The plume boundary displays extremely sharp interfaces (including thermal, salinity, and turbidity contrasts) with adjacent water masses. The boundary of the plume is not straight and regular but commonly shows numerous perturbations, often at regularly spaced intervals along the boundary (Figure 6). Note that some protrusions have very ragged edges, whereas others have smooth edges. At the present time it is uncertain whether these zones are residual effects advected seaward from a generation point near the mouth or whether they reflect continual regeneration at periodic intervals from the mouth. Closely spaced imagery flights during only one mission indicated that the forms advanced with velocities which averaged 0.5 meter/sec. In most instances these protrusions can be seen continuing across the plume and show up on color infrared imagery as alternating zones of low and high turbidity and in thermal images as alternating zones of warm and cool water, suggesting partial surface emergence of underlying warm seawater. The bands are normally separated by intervals of 250 to 450 meters and occur at both flooding and ebbing phases of the tide and at all river stages.

Low-altitude thermal imagery within the plume boundaries also disclose a series of thin wavelike forms (Figure 7A) that have lengths that range from 50 meters to 150 meters. These features occur only within the plume and are most commonly seen near the seaward termination of the plume boundary. They are most conspicuous on the thermal imagery, where they correspond to differing surface temperatures, but

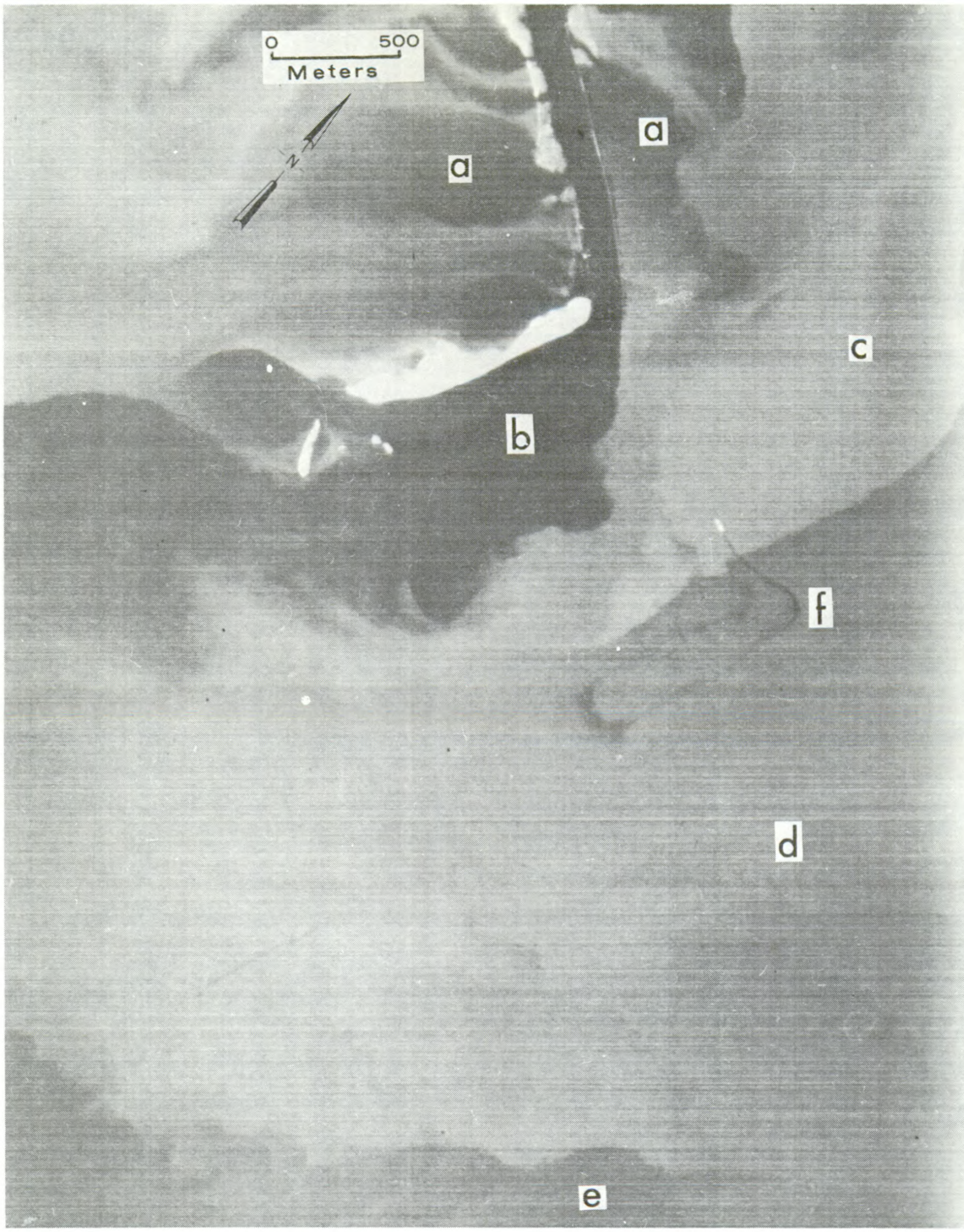

Figure 6 — RS14 thermal infrared scanner (8-14μ spectral band) image of South Pass taken during ebbing tide (1600 hours May 16, 1972) from an altitude of 5,000 meters. Lighter tones indicate warmer temperatures. a—Effluent debouching from breaks in main river channel; b—major freshwater plume issuing from South Pass; c—ambient fresh to brackish water mass; d—freshwater effluent plume from channel to the east; e—saline gulf water; f—boat wake.

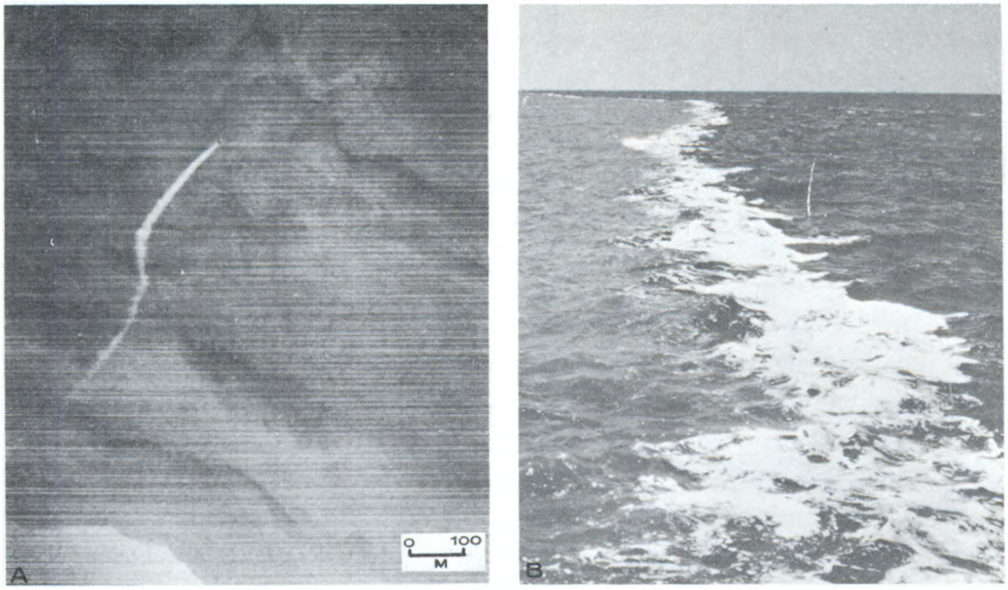

Figure 7 — A—Low-altitude (500 meters) RS14 thermal infrared scanner image showing details of the water structure in the effluent plume. Note the wave-like forms that exist. B—Ground photograph of boundary between two water masses. Fresh to brackish turbid water is to the left and clear saline gulf water is to the right.

occasionally they can be distinguished by varying turbidity concentrations in some color infrared imagery. The intense bending and contortions seen in Figure 7A are the result of boat wakes that passed through the area approximately 30 minutes prior to the flight. Note the one wake, generated by a small shrimping boat, present in the image. The turbulence from the boat is bringing warm, saline gulf water to the surface, indicating the thin nature of the freshwater plume.

The water mass labeled "c" in Figure 6 is the ambient fresh-brackish water issuing out of the numerous small river mouths east of the main river channel. The water mass labeled "d" (Figure 6) is a freshwater effluent plume from a major river mouth just off the image to the east. The boundary between water masses "c" and "d" is primarily a temperature gradient inasmuch as the shallow waters in the bays (water mass "c") are heated by constant mixing and form a major temperature contrast when they encounter the river plumes. Turbidity and salinity differences are normally minor.

The boundary between saline gulf waters (labeled "e" in Figure 6) and the ambient fresh-brackish water ("c" and "d", Figure 6) quite often displays the sharpest boundary present at the river mouth. This is particularly true during flooding tide. Turbidity contrasts are always great, as can be seen in the photograph (Figure 7B). The turbid brackish water is to the left, and the clear, saline gulf water is to the right. Quite often, large schools of fish are seen along this interface. Temperature differences are not extreme, commonly being only 1/2 to 1°C between the two water masses. The significant turbidity contrast between these to water masses can be seen in the high-altitude infrared imagery shown on the picture.

Thus at a river mouth several types of density gradients exist and constantly change their plan and profile geometry with changing oceanographic and riverine conditions. These interfaces could and do present problems to sonar operations. The presence of an interface between the transmitter and the target could reflect false targets or completely hide a target on the adjacent side of the interface. Quite often these interfaces are characterized by accumulations of trash (leaves, twigs, flocculated clays, *etc.*) and are highly charged with gases generated by temperature differences. All of these features reduce the efficiency of sonar. On the other hand, a knowledge of these interfaces can be utilized to strengthen the energy of transmitted signals and, if used properly, can assist in sonar searches. Although significant advances have been made in understanding the mechanisms that control these interfaces, more research is needed to allow reliable predictions of their changing shape and three-dimensional geometry.

References

1. Pritchard, D. W., "Estuarine Circulation Patterns," *Proc. Am. Soc. Cihil Engrs.,* 81, 717 (1955).
2. Ippen, A. T., and G. B. Keulegan, "Salinity Intrusions in Estuaries," in *Evaluation of Present State of Knowledge of Factors Affecting Tidal Hydraulics and Related Phenomena,* C. F. Wicker, ed., Chapter IV, U.S. Army Corps of Engrs., Committee on Tidal Hydraulics (1965).
3. Bates, C. C., "Rational Theory of Delta Formation," *Bull. Am. Assoc. Petroleum Geologists,* 37, 9, 2119-2161 (1953).
4. Wright, L. D., "Circulation, Effluent Diffusion, and Sediment Transport, Mouth of South Pass, Mississippe River Delta," *Coastal Studies Inst., Tech. Rept.* 84, La. State Univ., 56 p. (1970).
5. Wright, L. D., and J. M. Coleman, "Effluent Expansion and Interfacial Mixing in the Presence of a Salt Wedge, Mississippi River Delta," *J. Geophysical Research,* 76, 36, 8649-8661 (1971).

(Continued from Page 8)

By means of this new facility, NRL investigators are now able to measure Doppler spectra in microwave backscattering from wind waves at 9.375, 23.9 and 70.1 gigahertz as a function of wind speed, fetch and radar depression angles.

These measurements have led to the identification of three types of wave systems that cause scattering. They are: (1) the dominant wind wave, which is the primary scatterer for angles within 20 degrees of normal incidence; (2) wave-breaking systems or white caps, and (3) small wave systems, which are responsible for the scattering at lower angles.

The wind-wave tank will soon measure bistatic and forward scattering measurements to identify other ocean surface disturbances which may scatter radar impulses.

On the Naval Research Reserve

Officially Activated Research Reserve Companies

The Research Reserve program is composed of 61 companies throughout the United States. The Naval Reserve Officers are qualified in the conduct and/or administration of scientific research, or in patent, trademark, and copyright matters. These officers are available in the event of national emergency to meet the needs of the Office of Naval Research and the Naval Establishment. Through the year the companies report on their activities and training programs.

FIRST NAVAL DISTRICT

TIME AND PLACE OF MEETING	COMMANDING OFFICER & MAIL ADDRESS
NRRC 1-1 1930, 1st & 3rd Mondays Room 4-270, M.I.T. 77 Massachusetts Avenue Cambridge, Massachusetts 02138	LCDR Alan G. CAMERON, USNR Rockland Road Carlisle, Massachusetts 01741
NRRC 1-2 1930, 1st & 3rd Wednesdays Room 114, Naval & Marine Corps Reserve Center, Fields Point Providence, Rhode Island 02905	LT Richard C. WILKINSON, USNR 62 Griffin Drive Warwick, Rhode Island 02886

THIRD NAVAL DISTRICT

1830, 1st & 3rd Thursdays 821 United Nations Plaza 46th & 1st Avenue New York, New York 10017	LT Patrick D. SORAN, USNR 169 Colonia Road Summit, New Jersey 07901
NRRC 3-2 1930, 2nd & 4th Mondays Merchant Marine Academy Kings Point, New York 11024	CDR John G. BUSHARIA, USNR 134 Madisonville Road Basking Ridge, New Jersey 07920
NRRC 3-4 2000, 2nd & 4th Mondays Harkness Hall, Room 314 University of Rochester Rochester, New York 14627	LCDR Robert C. PIWKO, USNR 22 Bent Oak Road Rochester, New York 14624

NRRC 3-5
2000, 1st & 3rd Thursdays
Hartford Electric Light Company
176 Cumberland Avenue
Wethersfield, Connecticut 06169

CDR Benny A. ANDERSON, USNR
11 Lakeview Street
East Hampton, Connecticut 06424

NRRC 3-7
2000, 2nd & 4th Thursdays
Naval Reserve Center
Scotia, New York 12302

LCDR Frederick G. BAILY, USNR
Jockey Street, R. D. No. 1
Ballston Spa, New York 12020

NRRC 3-8
1900, 2nd & 4th Tuesdays
Young & Rubican, Inc.
6th Floor, 285 Madison Avenue
New York, New York 10017

CDR Arthur J. MORR, USNR
32 Grace Avenue
Lynbrook, New York 11563

NRRC 3-9
1930, 2nd & 3rd Wednesdays
Brookhaven National Laboratory
Upton, Long Island, New York 11973

LCDR William J. SCHNEIDER, USNR
6 Shaker Hollow Rd., Box 374
Setauket, New York 11785

NRRC 3-18
1945, 1st & 3rd Tuesdays
Naval Reserve Center
Onondaga Lake Parkway
Liverpool, N. Y. 13088

LCDR James E. KUNEMAN, USNR
309 Juanita Drive
Liverpool, New York 13088

FOURTH NAVAL DISTRICT

NRRC 4-1
2000, 1st & 3rd Wednesdays
FMC Corp. Research Center
US No. 1
Princeton, New Jersey 08540

CDR Earl K. SNEDEKER, Jr., USNR
160 Carter Road
Princeton, New Jersey 08540

NRRC 4-3
2000, 2nd & 4th Mondays
Naval & Marine Corps Reserve Center
4902 Forbes Avenue
Pittsburgh, Pennsylvania 15213

LCDR Robert S. HOWARD, USNR
3831 Logans Ferry Road
Pittsburgh, Pennsylvania 15239

NRRC 4-4
1930, Mondays
316 Wagner Building
Pennsylvania State University
University Park, Pennsylvania 16801

LCDR Carl R. AMICK, USNR
125 S. Osmond Street
State College, Pennsylvania 16801

NRRC 4-5
2000, Alternate Mondays
Naval & Marine Corps Reserve Center
3920 Kirkwood Highway
Wilmington, Delaware 19808

CDR Herbert W. LARSON, USNR
8 Hollingsworth Drive
Wilmington, Delaware 19807

NRRC 4-7
1930, Alternate Thursdays
(No meeting during July & Aug.)
Battelle Memorial Institute
Conference Room D
505 King Avenue
Columbus, Ohio 43201

LCDR Raymond E. MESLOH, USNR
6640 Guyer Street
Worthington, Ohio 43085

NRRC 4-8
1800, 2nd & 4th Wednesdays
Naval & Marine Corps Reserve Center
1089 East Ninth Street
Cleveland, Ohio 44114

LT David B. SNOW, USNR
24455 Lake Shore Blvd., Apt. 618E
Euclid, Ohio 44123

NRRC 4-11
1900, 1st, 2nd & 3rd Tuesdays
GE Technical Training Center
Interstate 75
Cincinnati, Ohio 45215

CDR Harold A. BALO, USNR
General Electric Company-Mail Drop A40
P. O. Box 196
Cincinnati, Ohio 45215

FIFTH NAVAL DISTRICT

NRRC 5-4
1945, 1st & 3rd Thursdays
Marine Corps Armory
Hamlet & Chesley Avenue
Baltimore, Maryland 21230

CDR Arthur B. CLAPSADDLE, USNR
227 Dawson Drive
Cockeysville, Maryland 21030

NRRC 5-8
2000, 2nd & 4th Thursdays
National Academy of Sciences
2102 Constitution Avenue, N.W.
Washington, D.C.

LCDR Melvin REICH, USNR
5102 Brentford Drive
Rockville, Maryland 20853

NRRC 5-9
1630, 1st & 3rd Fridays
(Except during First Quarter;
meetings are alternate Wednesdays)
Naval Research Laboratory
4555 Overlook Avenue
Washington, D.C. 20390

LCDR David J. NAGEL, USNR
4313 12th Road South, Apt. 21
Arlington, Virginia 22204

NRRC 5-10
2000, 2nd & 4th Tuesdays
Naval Medical Research Institute
National Naval Medical Center
Bethesda, Maryland 20014

LCDR C. Richard VAN NIEL, USNR
11104 Powder Horn Drive
Potomac, Maryland 20854

NRRC 5-11
2000, 1st & 3rd Tuesdays
Michelson Hall, Room 316
Naval Academy
Annapolis, Maryland 21402

CDR William J. THOMPSON, USNR
500 Old Pasture Lane
Severna Park, Maryland 21146

NRRC 5-12
1630, 2nd & 4th Mondays
Bldg. 1200, Rm. A135
Naval Weapons Laboratory
Dahlgren, Virginia 22448

LCDR David S. MALYEVAC, USNR
Box 149
Dahlgren, Virginia 22448

SIXTH NAVAL DISTRICT

NRRC 6-1
1930, 1st, 2nd & 3rd Thursdays
(No meetings during July & Aug.)
Naval & Marine Corps Reserve Center
274 Fifth Street, N.W.
Atlanta, Georgia 30318

CDR Raynor F. ALDEN, USNR
4008 Commodore Drive
Chamblee, Georgia 30341

NRRC 6-3
1930, 2nd & 4th Wednesdays
Army Reserve Training Center
Oak Ridge, Tennessee 37830

LCDR William C. MC WHORTER, USNR
112 Culver Road
Oak Ridge, Tennessee 37830

NRRC 6-6
1830, Mondays
(No meetings during July & Aug.)
NROTC Bldg., Univ. of N. C.
Chapel Hill, North Carolina

LCDR Jerry L. HARRIS, USNR
922 Green Street
Durham, North Carolina 27701

NRRC 6-8
1930, 1st, 3rd & 5th Mondays
Naval Reserve Center
Livingston & Parramore Streets
Orlando, Florida

LCDR Robert L. WALSH, USNR
169 Plumosus Drive
Altamonte Springs, Florida 32701

NRRC 6-9
1900, 1st, 3rd & 4th Mondays
Soil Test Laboratory
2400 College Station Road
Athens, Georgia 30601

CDR J. Benton JONES, USNR
115 Sweet Gum Drive
Athens, Georgia 30601

NRRC 6-17
1900, Mondays
Naval Reserve Center
203 Leeman Ferry Road, S.W.
Huntsville, Alabama

LCDR Russell JACKSON, USNR
2403 Bankhead Parkway, N.E.
Huntsville, Alabama 35801

NRRC 6-18
1930, 1st & 3rd Mondays
School of Engineering
Vanderbilt University
Nashville, Tennessee

LCDR Larry K. WILSON, USNR
1115 Grandview Drive
Nashville, Tennessee 37204

NRRC 6-19
1930, 1st, 2nd & 3rd Thursdays
Naval Reserve Center
12 Meadow Street
Chattanooga, Tennessee 37405

LCDR William R. CAUTHEN, USNR
1115 Tamarack Trail
East Ridge, Tennessee 37412

EIGHT NAVAL DISTRICT

NRRC 8-1
1930, Alternate Tuesdays
Richardson Memorial Building
Room 203, Tulane University
6823 St. Charles Avenue
New Orleans, Louisiana 70118

CDR Stanley P. KOLTUN, USNR
5601 Avron Boulevard
Metairie, Louisiana 70003

NRRC 8-3
1930, Mondays
Petroleum Engineering Building
Texas A&M College
College Station, Texas 77843

LCDR Robert G. MERRIFIELD, USNR
1403 Glade St.
College Station, Texas 77843

NRRC 8-4
1930, 1st & 3rd Wednesdays
Naval Reserve Center
Houston, Texas 77025

CDR Clay W. G. FULCHER, USNR
18710 Point Lookout
Houston, Texas 77058

NRRC 8-7
1930, Mondays
NROTC Building
University of New Mexico
Albuquerque, New Mexico 87106

LCDR Herbert H. HUGHES, USNR
7112 Lantern Road, N.E.
Albuquerque, New Mexico 87109

NRRC 8-9
1700, 1st & 3rd Tuesdays
Lecture Room Administration Bldg.
Los Alamos Scientific Laboratory
Los Alamos, New Mexico 87544

LT Emmett L. BRAZIER, Jr., USNR
P.O. Box 100
2177 43rd Street
Los Alamos, New Mexico 87544

NRRC 8-12
2000, 1st & 3rd Tuesdays
Santa Fe Building
114 Commerce Street
Dallas, Texas 75202

LCDR Paul D. MAYCOCK, USNR
204 Shadywood Lane
Richardson, Texas 75080

NRRC 8-13
1930, 2nd, 3rd & 4th Thursdays
Naval Reserve Center
701 E. 12th Street
Stillwater, Oklahoma 73105

CDR Franklin D. WICKS, USNR
2300 Meadowbrook
Ponca City, Oklahoma 74601

NINTH NAVAL DISTRICT

NRRC 9-1 1900, 2nd & 4th Tuesdays Naval Armory Randolph at the Lake Chicago, Illinois 60601	CDR John C. SIEBERT, USNR 1646 N. Sedgwick Chicago, Illinois 60614
NRRC 9-3 1930, Mondays (Varied dates July, Aug. Sept.) 62 North Hall, Univ. of Michigan Ann Arbor, Michigan 48104	LCDR William C. PRINCE, USNR 2312 Walter Drive Ann Arbos, Washington 48103
NRRC 9-4 2000, 2nd & 4th Tuesdays Naval & Marine Corps Reserve Center Milwaukee, Wisconsin 53207	CDR Bruce E. SNYDER, USNR 12007 Elmhurst Parkway Wawautosa, Wisconsin 53226
NRRC 9-5 1900, 1st, 2nd & 3rd Wednesdays NROTC Building Iowa State College Ames, Iowa 50010	LCDR Charles R. MISCHKE, USNR 1815 Maxwell Avenue Ames, Iowa 50010
NRRC 9-6 1930, 2nd & 4th Mondays Room 208, Mechanical Eng. Bldg. University of Minnesota Minneapolis, Minnesota 55414	LCDR John W. BARBER, USNR 1919 Hunterlane St. Paul, Minnesota 55118
NRRC 9-10 2000, Thursdays Naval Reserve Center Building 512 Great Lakes, Illinois 60088	CDR Ralph I. LYTLE, USNR 252 Ravine Forest Drive Lake Bluff, Illinois 60044
NRRC 9-12 1930, Thursdays Agriculture Bldg., Room 112 Colorado State University Ft. Collins, Colorado 80521	LCDR William M. HANTSBARGER, USNR 2712 Killdeer Drive Ft. Collins, Colorado 80521
NRRC 9-16 1930, Mondays 221 Computing Center Michigan State University East Lansing, Michigan	LCDR Oscar TABOADA, USNR 1826 N. Hayford Avenue Lansing, Michigan 48912
9-21 1930, 1st & 2nd Tuesdays Denver Federal Center Denver, Colorado 80225	LCDR Robert D. PRICE, USNR 370 Auburn Street Boulder, Colorado 80303

9-23
1930, 2nd & 4th Wednesdays
Argonne National Laboratory
Argonne, Illinois 60439

LCDR John E. BAUBLITZ, USNR
1449 Arrow Wood Lane
Downers Grove, Illinois 60515

NRRC 9-28
1900, Wednesdays
NROTC Armory
6th Street & Stewart Road
Columbia, Missouri 65201

LT Larry J. PERRY, USNR
303 Corprew
Fayette, Missouri 65248

ELEVENTH NAVAL DISTRICT

NRRC 11-2
2000, 1st & 3rd Mondays
Naval & Marine Corps Reserve Center
2727 Paloma Street
Pasadena, California 91107

LCDR Jack H. BURTHE, USNR
P. O. Box 511
West Covina, California 91790

NRRC 11-5
1930, 2nd, 3rd & 4th Tuesdays
Naval Reserve Center
San Diego, California 92133

LCDR Thomas J. DE LACY, USNR
1427 Big Red Road
Alpine, California 92001

NRRC 11-7
2000, 1st, 2nd & 3rd Thursdays
Naval & Marine Corps Reserve Center
1000 S. Alvernon Way
Tucson, Arizona 85711

LCDR Gordon O. PRICKETT, USNR
4149 E. Holmes Street
Tucson, Arizona 85711

NRRC 11-11
1930, Mondays
Naval & Marine Corps Reserve Center
3400 Airport Avenue
Santa Monica, California 90405

LCDR Henry J. BENDER, USNR
666 East Ocean Boulevard
Long Beach, California 90069

TWELFTH NAVAL DISTRICT

NRRC 12-2
1700, 1st, 2nd & 3rd Mondays
Room 118, Building 311
Lawrence Radiation Laboratory
Livermore, California

CDR Thomas E. Bloom, USNR
1221 Diablo Way
San Jose, California 95120

NRRC 12-3
1930, 1st & 3rd Wednesdays
Lockheed Missile & Space Co.
Building 181
Sunnyvale, California 94000

LCDR Petter W. KNOPF, USNR
927 Paradise Way
Palo Alto, California 94306

NRRC 12-5
1930, 2nd & 4th Wednesdays
Room 246, Cory Hall
University of California
Berkeley, California 94707

CDR Howard A. JAMES, USNR
531 Vincente Avenue
Berkeley, California 94707

NRRC 12-6
1930, 1st, 2nd & 4th Thursdays
Conference Room, 197 Briggs Hall
University of California
Davis Medical School
Davis, California 95616

CDR David R. STROM, USNR
58 College Park
Davis, California 95616

NRRC 12-8
2000, 2nd, 3rd & 4th Wednesdays
Room S-136, Spanagel Hall
Naval Postgraduate School
Monterey, California

CDR Allen E. FUHS, USNR
25932 Carmel Knolls Drive
Carmel, California 93921

THIRTEENTH NAVAL DISTRICT

NRRC 13-1
1930, 1st, 3rd & 4th Mondays
Naval Reserve Center
860 Terry Avenue, North
Seattle, Washington 98109

LCDR Frederick P. CARLSON, USNR
12701 6th Avenue, N.W.
Seattle, Washington 98177

NRRC 13-4
2000, 1st, 3rd & 4th Tuesdays
Naval & Marine Corps Reserve Center
Swan Island
Portland, Oregon 97217

CDR James W. REAM, USNR
10915 S.W. 57th Avenue
Portland, Oregon 97219

NRRC 13-5
1930, 1st & 3rd Mondays
NROTC Armory
Oregon State University
Corvallis, Oregon 97330

CDR Joe B. ZAERR, USNR
5945 N.W. Rosewood Drive
Corvallis, Oregon 97330

Navy Successfully Tests Large Object Salvage System

The Navy has recently completed three weeks of successful open sea testing of a newly developed Large Object Salvage System (LOSS) which lifted a 100 ton object from 100 feet of water in the Gulf of Mexico off Panama City, Florida. Termed "LOSS," the system now consists of a large pontoon which is lowered over the sunken object, attaches arms to the object by firing explosive studs and through new bouyant gas generating techniques raises the object to the surface. The latter two steps are accomplished by remote control, from a surface support ship.

When development is complete, LOSS will have a self positioning pontoon and, through use of multiple pontoons, will be able to lift aircraft and medium hull ships from depths of 1000 feet. Presently a single pontoon can lift 100 tons. Though divers are now required to attach guidelines from the support ship to the pontoon to the sunken object, the completed system will eliminate use of divers.

The LOSS pontoon, which is 45 feet long by 15 feet diameter, is an intricate system of electronic controls, high-pressure valves and gas generating equipment. The pontoon system is controlled from a command center aboard a surface support ship, thus minimizing the complex surface support presently required for such operations. Single and multiple pontoons can be towed to the salvage site by the surface support ship.

To raise a 100 ton object and a pontoon—which itself weights 100 tons—to the surface requires building up a gas bubble inside the pontoon large enough to displace a weight of water equivalent to the combined weights of the pontoon and object. Large Object Salvage System generates the required gas bubble by any one of three methods. For shallow depths of 300 to 400 feet the conventional compressed air technique is used where compressed air is supplied to the pontoon from a surface support ship. For deeper depths two new gas generating techniques were proved in the recent at-sea tests. These two different gas generating techniques were a cryogenic (super cold) system utilizing liquid nitrogen (LN2) to produce gaseous nitrogen and a liquid rocket fuel system ulitizing hydrazine (H2H4) to produce hydrogen.

The three different methods of providing pontoon buoyancy are necessary to ensure a lift capability over a large range of depths. Near the surface, whenever compressed air lines from a surface support ship can be utilized, this method will prove most effective. Liquid nitrogen in special containers (Dewar flasks) becomes the best buoyant agent at depths beyond surface support to depths where the pressure of water becomes too great to generate gaseous nitrogen (2,000 to 3,000). Beyond this depth, hydrazine becomes the most efficient gas generating technique.

This project is part of an overall Ocean Engineering Research and Development program coordinated by the Oceanographer of the Navy, and managed by the Naval Ship Systems Command as the Principal Development Activity. In addition to the salvage project, the other Ocean Engineering R&D efforts include manned and unmanned submersible vehicles, oceanographic instruments, swimmer and diver equipment and systems, and ocean bottom construction and placements systems.

Primary performing activities involved in the LOSS development include: the Naval Coastal Systems Laboratory, Panama City, Florida, the lead development activity; the Naval Civil Engineering Laboratory, Port Hueneme, California, developer of the hydrazine gas generating system; and Battelle Memorial Institute, Columbus, Ohio, engineering support. Other participants included: Murphy-Pacific Inc., the U.S. Navy Safety Center and the Naval Combat Action Camera Group.

Research Notes

Navy Satellite Experiment Records Major Solar Flare Effects

For the first time a Navy satellite experiment has closely monitored and recorded from beginning to end the effects produced in the earth's ionosphere by a major solar flare that lasted several days. The flare, which occurred in early August, bathed the earth's polar regions in the exotic light of Aurora Borealis (Northern Lights) and interrupted worldwide radio communications for a time.

The Agena satellite, which was placed in a 400-mile circular polar orbit last October, contains four experimental packages as part of the Department of Defense Space Test Program. The instrument package designed to measure ionospheric changes including those caused by solar flares was built by Lockheed's Palo Alto Research Laboratory under an Office of Naval Research contract, with funds provided by the Defense Nuclear Agency.

The satellite vehicle itself was designed and constructed by the Air Force Space and Missile Systems Organization (SAMSO). SAMSO launched the satellite from Vandenburg Air Force Base, California, on October 17 using a Thor-Agena rocket. It is expected to remain operational for up to a year.

A preliminary look at data sent by the satellite shows that the giant solar flare resulted in a more intense bombardment of the earth by showers of electrons and protons, called plasmas, than any previously watched by satellites. Since we are now in the declining portion of the 11-year solar activity cycle, fewer solar flares are expected. Scientists believe, however, that those that occur in this period will be of larger magnitude.

The solar storm began on August 3 and the high-energy particles hit the earth's atmosphere within a few hours. The slower-moving plasma particles arrived in about four days. The highly valuable data collected from the perspective of space will enable Navy scientists to significantly increase our understanding of the effects of solar storms on polar radio communications, auroral and polar cap phenomena.

Dr. Robert T. Johnson, a Lockheed scientist, said there are indications that at the peak of the flare, absorption of 30 mega-hertz radio waves in the polar regions amounted to 18 decibles (DB), which is the largest radio wave absorption observed at that frequency in the past 11 years. Dr. Johnson, supported by the Office of Naval Research, has been watching solar storm effects by means of satellite experiments since 1962.

Aside from possibly two European satellites, plus whatever the Russians may have in space, the Navy experiment is believed to be the only one in polar orbit capable of monitoring the sun-produced ionospheric disturbances.

The experiment on the satellite is in two parts—the low and high energy particle detectors and the Earth-Reflecting Ionospheric Sounder (ERIS). The experiment has 18 individual instruments to collect data on proton, alpha and electron particles that come from the sun and enter the upper atmosphere.

ERIS sends out high frequency radio signals in the polar regions and then receives and records the signals reflected back from the earth's surface to the satellite. These signals are partially absorbed in the upper atmosphere because of the ionizing effect of the high energy particles from the sun.

Observations made from the Navy experiment aboard the Agena may shed additional light on ionospheric phenomena that have puzzled man for centuries.

NRL Scientists Solve Overheating Problems in Satellite Solar Cells

Two scientists at the Naval Research Laboratory (NRL) have improved the operating efficiency of satellite power systems by devising new techniques to prevent overheating of the solar cells. Long-range effects of their innovation could include extending the life expectancy of future satellites.

Richard L. Statler and Dr. Bruce J. Faraday, research physicists of the Laboratory's Nuclear Sciences Division, developed their techniques for upgrading satellite performance by fabricating solar panels of unique materials which allow cooler operations thus increasing satellite power and performance. These techniques relate to the heart of all man-made orbiting bodies—the power subsystems.

Solar cells absorb 90 percent of the incident solar energy, but are able to convert only 12 percent to electrical power. The remainder normally heats up the solar cell, reducing its efficiency by as much as 30 percent. This heat buildup in the solar cell has been avoided by the new NRL cooling techniques, resulting in higher efficiency.

Faraday and Statler's techniques, which have already been incorporated on NRL satellites built by the Space Systems Division, not only provide for an increase in available power, but also permit a savings in satellite weight, thereby leaving more room for additional experiments. These improvements in satellite technology also promise significant cost savings for building and operating solar cell power supply subsystems.

Computerized Design for Miniature Microwave Components

The Naval Research Laboratory's Electronics Division has developed a computer-aided method for designing broadband directional couplers as a miniature microwave component using planar transmission lines on high dielectric ceramic materials.

Until now, the development of broadband couplers that use such structures has been impeded by an inability to attain sufficiently tight coupling with coupled-line configurations that lend themselves to standard thin-film fabrication techniques.

The NRL method, programmed in Fortran IV for use on the CDC 3800 digital computer at the NRL Computation Center, uses a moment solution to compute the impedance and phase velocity for each of the even and odd modes of an arbitrary configuration of coupled transmission lines. Dielectric inhomogeneities in the system are handled in this treatment.

One of several directional couplers developed by this technique was fabricated on a 2 × 1 × 0.025-in. portion of alumina substrate by using thin-film techniques. The cross section of the coupled region of this device in Figure 1(a) employs a version of coupled microstrip lines with the ground plane width being finite and reduced, compared to that used in standard edge-coupled microstrip shown in Figure 1(b).

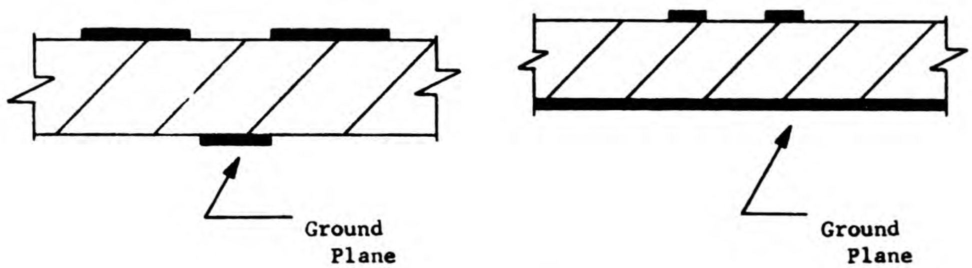

(a) Reduced ground plane width   (b) Standard ground plane width

Configurations of coupled microstrip lines

DSRV-2

The DSRV (Deep Submergence Rescue Vehicle) is a new concept in submarine rescue which will vastly extend the rescue capability in-so-far as depth of water is concerned. Unlike previous rescue systems, when the DSRV is launched from the support ship, it is a totally independent unit, capable of locating, mating with, and receiving up to 24 men from a distressed submarine.

The DSRV can be loaded, with its support equipment, onboard three 0-141 aircraft and flown to a port nearest a distressed submarine. At that port, the DSRV can be loaded aboard a "Mother Submarine" or an ASR (Submarine rescue ship) and transported to the scene of operations. When the DSRV is carried "Piggy Back" on a mother submarine, the submarine becomes an underwater base to which the DSRV transfers personnel from a disabled submarine.

The DSRV is 49 feet long, 8 feet in diameter, and propelled by electric motors and batteries. It has an operating depth of 3500 feet; however, during testing DSRV-2 has been submerged to a depth of 5280 off San Diego, California.

Propulsion and control of the DSRV are achieved by a conventional stern propeller in a movable control shroud, and horizontal and vertical directed thrusters located forward and aft on the craft. This permits the DSRV to mate with a submarine at angles to 45 degrees from the horizontal and the vertical approach.

The DSRV's outer hull is made of fiberglass. There are three interconnected spheres which form the manned pressure capsule. Each sphere is 7-1/2 feet in diameter and is constructed of HY-140 steel. The forward sphere contains the vehicles's control equipment and is manned by the operator and co-operator. The mid and aft spheres can accommodate 24 passengers and a third crewman.

DSRV-2 is the second such deep submergence rescue vehicle to be placed in operation by the Navy. In addition, it represents the second such rescue

U. S. GOVERNMENT PRINTING OFFICE : 1972 O - 486-913

submarine in the world. Admiral Elmo R. Zumwalt, the Chief of Naval Operations, has reaffirmed that, upon request, all information required to modify the submarines of any other nation to permit DSRV rescue will be willingly provided. When DSRV-2 joins the Fleet after an extensive test and evaluation period it will be part of the Navy's inventory of search and rescue assets available for international emergencies.

Improved Traveling Wave Tubes for Microwave System Amplifiers

Scientists at the Naval Research Laboratory have designed and operated a broadband cross flow, fluid cooled, helix traveling wave tube, used in microwave amplifiers for continuous wave radio-frequency signals, to an average power of over 5 kilowatts or 5,000 watts.

The 5 kilowatt average power output from the new development represents about twice that of other octave bandwidth tubes under development, and is expected to enhance microwave systems used for communications and other purposes. It should be possible to run the tube at 10KW peak with a 50% duty cycle, which is considered a great improvement over those presently in use.

There has long been a need for microwave amplifiers capable of amplifying continuous wave radio-frequency signals to levels of several kilowatts over broad frequency bands. The new development is expected to answer most of these problems and establish the feasibility of a new traveling wave tube technique for many electronic uses.

The principal investigators for the present development are Dr. Sidney T. Smith and Lester M. Winslow. Dr. Smith is the head of the Electron Physics Branch and Mr. Winslow is the head of the Traveling Wave Tube Section.

NAVAL RESEARCH REVIEWS publishes highlights of research conducted by Navy laboratories and contractors and describes important naval experimental facilities. Manuscripts submitted for publication, correspondence concerning prospective articles, and changes of address, should be directed to Code 109, Office of Naval Research, Arlington, Va. 22217. Requests for subscriptions should be directed to the Superintendent of Documents, U.S. Government Printing Office, Washington, D.C., 20402. Subscription price: $1.75 per year in the U.S. and Canada; $2.25 per year, foreign; $0.20 per individual copy. The issuance of this periodical approved in accordance with Dept. of the Navy publications and printing regulations.

Editor: WILLIAM J. LESCURE

NAVSO P-510

Associate Editors:

A. R. LAUFER, ONR PASADENA

A. R. DAWE, ONR CHICAGO

A. L. POWELL, ONR BOSTON

D. A. PATTERSON, NAVAL RESEARCH LABORATORY

IN THIS ISSUE

VOL. XXV, NO. 10

Caption for Cover Picture

A high-altitude (20,000 meters) photograph of some of the mouths of the Mississippi River. The distinct water masses (labeled on the photo) are apparent on the image; these can be attributed predominately to turbidity, but each boundary also displays salinity and temperature differences. See article on page 9.

DEPARTMENT OF THE NAVY
OFFICE OF NAVAL RESEARCH
ARLINGTON, VA. 22217

OFFICIAL BUSINESS

PENALTY FOR PRIVATE USE, $300.

POSTAGE AND FEES PAID
DEPARTMENT OF THE NAVY
DoD-316

U.S.MAIL